Dynamics of the Core Tryptophan during the Formation of a Productive Molten Globule Intermediate of Barstar †

ARTICLE *in* BIOCHEMISTRY · AUGUST 2003

Impact Factor: 3.02 · DOI: 10.1021/bi030006b · Source: PubMed

3 AUTHORS, INCLUDING:

Jayant B Udgaonkar
Tata Institute of Fundamental Research
147 PUBLICATIONS **4,286** CITATIONS

Dynamics of the Core Tryptophan during the Formation of a Productive Molten Globule Intermediate of Barstar†

Bhadresh R. Rami,‡ G. Krishnamoorthy,§ and Jayant B. Udgaonkar*,‡

National Centre for Biological Sciences, Tata Institute of Fundamental Research, GKVK Campus, Bangalore 560065, India, and Department of Chemical Sciences, Tata Institute of Fundamental Research, Mumbai 400005, India

Received January 3, 2003; Revised Manuscript Received April 17, 2003

ABSTRACT: The evolution of the nanosecond dynamics of the core tryptophan, Trp53, of barstar has been monitored during the induction of collapse and structure formation in the denatured D form at pH 12, by addition of increasing concentrations of the stabilizing salt Na_2SO_4. Time-resolved fluorescence methods have been used to monitor the dynamics of Trp53 in the intermediates that are populated during the salt-induced transition of the D form to the molten globule B form. The D form approximates a random coil and displays two rotational correlation times. A long rotational correlation time of 2.54 ns originates from segmental mobility, and a short correlation time of 0.26 ns originates from independent motion of the tryptophan side chain. Upon addition of ∼0.1 M Na_2SO_4, the long rotational correlation time increases to ∼6.4 ns, as the chain collapses and the segmental motions merge to reflect the global tumbling motion of a pre-molten globule P form. The P form exists as an expanded form with ∼30% greater volume than the native (N) state. The persistence of an ∼50% contribution to anisotropy decay by the short rotational correlation time suggests that the core of the P form is highly molten and permits free rotation of the Trp side chain. With increasing salt concentrations, tight core packing is achieved before secondary and tertiary structure formation is complete, an observation which agrees well with earlier kinetic folding studies. Thus, the equilibrium model developed here for describing the formation of structure during folding faithfully captures snapshots of transient kinetic intermediates observed on the folding pathway of barstar. A comparison of the refolding kinetics at pH 7, when refolding is initiated from the D, P, and B forms, suggests that formation of a collapsed state with a rigid core and ∼30% secondary and tertiary structure, which presumably defines a coarse native-like topology, constitutes the intrinsic barrier in the folding of barstar.

Transfer of information from the linear sequence of amino acids in a polypeptide chain to the unique three-dimensional structure of a protein defines the process of protein folding. For many proteins, the folding process occurs in multiple stages. The process of information transfer can then be analyzed by critically studying each step in the folding process. Kinetic intermediates are, however, short-lived and are not easily amenable to detailed structural characterization. Several proteins populate partially structured forms, commonly termed molten globule (MG) forms, at equilibrium under diverse solvent conditions (*1*−*3*). MG forms possess structural features that are intermediate between the native and the unfolded forms. The extent of similarity between an equilibrium MG and its kinetic counterpart, and the relevance of a kinetic intermediate in directing the conformational search during the folding process, are issues of intense debate and research (*4*−*9*).

The MG is envisaged as an ensemble of highly dynamic, interconverting forms whose average properties include (a) considerable secondary structure, (b) few or no tertiary contacts, (c) solvent-exposed hydrophobic patches, and (d) near-native dimensions. MG-like forms, both kinetic (*10*−*15*) and equilibrium (*16*−*21*), have been suggested to play productive roles in the folding of proteins, and their relevance has been validated further by theoretical studies (*16*, *22*−*24*). The mechanism of formation of a MG from an unfolded protein is poorly understood, and the placement of the MG with respect to the folding transition state is not clear. An understanding of the physical forces that drive the U → MG transition, and an understanding of the structures, energetics, and dynamics of forms populated during this transition, will help in better delineating the folding process.

The hydrophobic cores of proteins are tightly packed with densities approaching those of crystals of organic compounds (*25*), and hydrophobic and packing interactions make a major contribution to the stability of the native state (*26*). Several proteins have been shown to fold via an initial hydrophobic collapse of the polypeptide chain (*27*−*34*). It is thought that the initial collapse is relatively nonspecific (*35*), and that the subsequent formation of specific packing interactions (*34*)

† This work was supported by the Tata Institute of Fundamental Research and the Department of Science and Technology, Government of India. B.R.R. is the recipient of the Kanwal Rekhi Scholarship for Career Development from the Kanwal Rekhi Foundation. J.B.U. is the recipient of the Swarnajayanti Fellowship from the Government of India.

* To whom correspondence should be addressed. E-mail: jayant@ncbs.res.in. Fax: 91-80-3636662.

‡ National Centre for Biological Sciences, Tata Institute of Fundamental Research.

§ Department of Chemical Sciences, Tata Institute of Fundamental Research.

10.1021/bi030006b CCC: $25.00
Published on Web 06/13/2003

with definite stereochemical requirements (*32*) occurs progressively in stable intermediates later during folding. What remains poorly understood is the role of the hydrophobic core during the folding process, as well as the extent to which formation of the core contributes to the rate-limiting barrier. Mutational studies coupled to Φ-value analysis suggest that a folding nucleus comprising critical core residues (*36*−*38*) might already have formed in the transition state for folding. It has been suggested that the evolution of a gross, dynamic, native-like topology that defines the transition state comprises the energetic barrier in folding (*39*−*43*). Does tight packing in the core play a role in determining the native-like fold in the transition state and in late folding intermediates? What role does it play in further development of structure? While both experimental (*44*−*46*) and theoretical studies (*47*−*49*) have suggested that the native fold determines packing, and that packing does not determine the native fold, very little is known about when, during the folding process, tight packing of the core is achieved.

To address some of these fundamental questions, this study carries forward, now through the application of time-resolved fluorescence lifetime and anisotropy measurements (*50*−*53*), earlier steady-state spectroscopic investigations of the salt-induced formation of structure in the high-pH denatured, D form of barstar (*21*). The highly sensitive fluorescence properties of Trp53 (*54*), buried completely in the hydrophobic core, have been exploited to provide valuable information about core solvation during the folding reaction. The use of high-resolution time-resolved fluorescence methods has permitted the evolution of local and global structural features of barstar to be monitored during folding, with the motional dynamics of Trp53 serving as a measure of the consolidation of the core during folding.

The earlier results had indicated that the equilibrium folding pathway can be summarized by the following mechanism (*21*):

$$D \rightleftharpoons P \rightleftharpoons I \rightleftharpoons B \rightarrow N$$

According to this mechanism, the fully unfolded D form at pH 12 undergoes a global collapse to the structure-less, pre-molten globule P form, with the addition of ∼0.1 M Na_2SO_4. With further addition of salt, the P form attains aspects of secondary and tertiary structure in a highly noncooperative manner, to finally attain the molten globule conformation (B) at 1 M Na_2SO_4 (pH 12). The tryptophan emission spectrum of the B form suggests that it is a dry molten globule with a solvent-excluded core. The noncooperative nature of the salt-induced structural transitions as monitored by multiple spectroscopic probes and urea denaturation profiles suggest that at least one intermediate populates the P ⇌ B transition. Kinetic refolding studies supported by simulations have shown the B form to be an on-pathway folding intermediate.

This study provides a detailed picture of how the protein core evolves during the formation of the on-pathway, molten globule intermediate, the B form. It is shown that the product of the initial collapse of the unfolded polypeptide chain, the pre-molten globule, P form, has a highly solvated, dynamic core. Compaction and consolidation of the core appear to be complete before secondary and tertiary structural features characteristic of the molten globule B form are attained. Kinetic refolding studies suggest that the formation of a collapsed state with a compact core, overlaid with ∼30% secondary and tertiary structure, constitutes the rate-limiting barrier to the folding process.

MATERIALS AND METHODS

Protein Expression and Purification. A single tryptophan (Trp53)-containing mutant form of barstar, W38FW44F, has been used for all the studies. The procedure for purification was similar to that described earlier for wild-type (*wt*) barstar (*55*). An extinction coefficient of 10000 M^{-1} cm^{-1} at 280 nm was used to estimate protein concentrations. The protein used for all experiments was >98% pure as estimated by SDS−PAGE. ESI-MS on a Micromass QTOF-Ultima spectrometer, using protein at a concentration of 20 μM, showed that the mass of the protein was 10 265 Da, which is consistent with the N-terminal methionine not being cleaved after synthesis.

Buffers. All chemicals used to make buffers were of the highest purity grade (Sigma Aldrich Inc.). Sodium phosphate was used for buffering at pH 7. Sodium tetraborate was used for buffering at high pH. The pH was adjusted using NaOH or HCl. Sodium sulfate was dissolved in 30 mM sodium tetraborate for a 1 M stock solution. All buffers included 250 μM EDTA and a 20−50-fold molar excess of DTT relative to the protein concentration. All buffers were passed through a 0.22 μm filter before being used.

All experiments were carried out at 25 °C, and a >10-fold concentration range to rule out aggregation artifacts. Experiments in the presence of Na_2SO_4 were carried out after the sample had been incubated for 2 h, and all the measurements were repeated at 24 h.

Steady-State Fluorescence Anisotropy Measurements. Steady-state anisotropy (r_{ss}) measurements were carried out by using a SPEX FluoroMax-3 spectrofluorometer. Anisotropy measurements were taken after excitation of the sample at 295 nm, and by monitoring the emission at 335 nm, at parallel and perpendicular polarizations independently. Great precaution and care were exercised in the measurement of the geometry (*G*) factor of the emission monochromator, which was calculated using a dilute scattering solution.

Light Scattering Measurements. Dynamic light scattering experiments were carried out on a DynaPro-99 unit (Protein Solutions Ltd.). Samples were incubated for 3 h in buffers at pH 12 containing 0−1 M Na_2SO_4. The samples were degassed, spun down at 14000 rpm for 15 min, and filtered through 0.02 μm filters. Data were acquired over 150 s, where each data point was averaged over 3 s at a sensitivity of 80%. All fluctuations in scattering intensities which were greater than 15% were excluded from data analysis. The DynaLS software (Protein Solutions Ltd.) was used to resolve the measurements into well-defined Gaussian distributions. The goodness of fit was verified by the residuals. Salt concentrations were confirmed by refractive index measurements.

Fluorescence Lifetime and Anisotropy Decay Measurements. Time-resolved fluorescence decay measurements were made employing a continuous-wave (CW) mode-locked frequency-doubled Nd:YAG laser-driven dye (Rhodamine 6G) laser that generates 4−10 ps pulses (*33*, *56*). The second harmonic output (295 nm) of an angle-tuned KDP crystal

was used to excite the protein sample, and the fluorescence emission was collected through a 320 nm cutoff filter followed by a monochromator. The filter prevents scattered light from reaching the detector. Scattered light is highly polarized ($r = 1$), and even a small percentage of it reaching the detector can cause significant changes in the anisotropy of dilute solutions. The peak counts obtained in the control experiments were comparable to the background level. In fluorescence lifetime measurements, the emission was monitored at the magic angle (54.7°) to eliminate the contribution from the decay of anisotropy. Fluorescence decay curves were obtained by using a time-correlated single-photon counting (TCSPC) setup coupled to a microchannel plate photomultiplier (model 2809U, Hamamatsu Corp.). The instrument response function (IRF) had a half-width of ~40 ps. The fluorescence decay curves at the magic angle were analyzed by deconvoluting the observed decay with the IRF to obtain the intensity decay function represented as a sum of multiple exponentials:

$$I(t) = \sum_i \alpha_i \exp\left(\frac{-t}{\tau_i}\right) \qquad i = 1-4 \tag{1}$$

where $I(t)$ is the fluorescence intensity at time t and α_i is the amplitude of the ith lifetime τ_i such that $\sum_i \alpha_i = 1$.

Anisotropy was calculated as

$$r(t) = \frac{(I_{||} - I_{\perp})G(\lambda)}{(I_{||} + 2I_{\perp})G(\lambda)} \tag{2}$$

where $I_{||}$ and $I_{\perp}$ are the emission intensities collected at polarizations parallel and perpendicular to the polarization of the excitation beam, respectively, and $G(\lambda)$ is the geometry factor at the wavelength of emission (λ). The G factor of the emission collection optics was determined in separate experiments using a standard sample (laser dye BMQ dissolved in ethanol) for which the rotational correlation time was 0.23 ns and the fluorescence lifetime was 0.83 ns. Intensity decays in the parallel and perpendicular channels were acquired for the protein at each salt concentration, and the parameters obtained upon analysis were averaged over three independent experiments. Time-resolved fluorescence decays were analyzed on the basis of the following model:

$$I_{||} = \frac{1}{3} I(t)[1 + 2r(t)] \tag{3}$$

$$I_{\perp} = \frac{1}{3} I(t)[1 - r(t)] \tag{4}$$

$$I(t) = \sum_i \alpha_i \exp\left(\frac{-t}{\tau_i}\right) \qquad i = 1-4 \tag{5}$$

$$r(t) = r_o \sum_j \beta_j \exp\left(\frac{-t}{\tau_{r_j}}\right) \qquad j = 1-2 \tag{6}$$

where $I_{||}$ and $I_{\perp}$ are the emission intensities collected at polarizations parallel and perpendicular to the polarization of the excitation beam, respectively. $I(t)$ is the total fluorescence intensity at time t. r_o is the initial anisotropy, and α_i and β_j are the amplitudes associated with the ith fluorescence lifetimes and jth rotational correlation times, respectively, such that $\sum \alpha_i = \sum \beta_j = 1$. In this model, each τ_i is associated with both τ_{r_1} and τ_{r_2}. Nonlinear least-squares analysis (Marquardt method) was performed to extract amplitude parameters α_i, β_i, lifetimes τ_i, and correlation times τ_{r_j}. $I_{||}$ and $I_{\perp}$ were analyzed globally by using the measured IRF (*53*). The G factor was calculated as described above. Since the goodness of fits were satisfactory with two correlation times (τ_{r_1} and τ_{r_2}), and did not improve with the addition of a third component, the number of τ_r components was kept at two. The best fit of the theoretical curve to the data was evaluated from the plot of weighted residuals, and the reduced χ^2 value. The steady-state fluorescence anisotropy (r_{ss}) was calculated from the parameters obtained from the time domain data by using eq 7:

$$r(t) = \frac{r_o \sum_i \sum_j \alpha_i \beta_j \left(\frac{1}{\tau_i} + \frac{1}{\tau_{r_j}}\right)^{-1}}{\sum_i \alpha_i \tau_i} \tag{7}$$

The average angular range of the hindered rotation of Trp53 was calculated by the model of isotropic diffusion inside a cone (*57*). The semiangle Θ of the cone was calculated as

$$\Theta = \cos^{-1}\left[{}^1/_2(\{[1 + 8(\beta_1)^{1/2}]^{1/2}\} - 1)\right] \tag{8}$$

where β_1 is the amplitude corresponding to the slow rotational correlation time, τ_{r_1}.

Viscosity Measurements. The viscosities of solutions at pH 7 and 12, containing different concentrations of Na_2SO_4, ranging from 0 to 1 M, were determined using an Ostwald viscometer thermostated at 25 °C. The relative viscosity was obtained by dividing the solution viscosity by the solvent viscosity. The values of the relative viscosity were used to correct the hydrodynamic radius obtained from the DLS measurements, and were also used to correct the values of the long rotational correlation time obtained from the time-resolved anisotropy measurements.

RESULTS

Fluorescence Lifetime Measurements. Earlier studies had shown that the lifetimes obtained by fitting the fluorescence intensity decay data to discrete exponentials agreed well with those obtained from the model free maximum entropy method (MEM) analysis (*53*). Here, the data have been analyzed by fitting the fluorescence intensity decays to discrete exponential functions. Figure 1a shows the fluorescence lifetime decay characteristics of Trp53 in W38FW44F under native conditions (pH 7). While the data can be fit to a single exponential, the goodness of fit increases significantly upon fitting to two exponentials with the major fluorescence lifetime decay component ($\tau_1 \sim 5.06$ ns) contributing to ~95% of the amplitude and the second component ($\tau_2 \sim 1.1$ ns) contributing to the remaining 5% of the amplitude (Table 1).

Figure 1b shows a representative trace for the fluorescence decay kinetics from the excited state of Trp53 in the U form in 6 M GdnHCl at pH 7. The data fit best to three

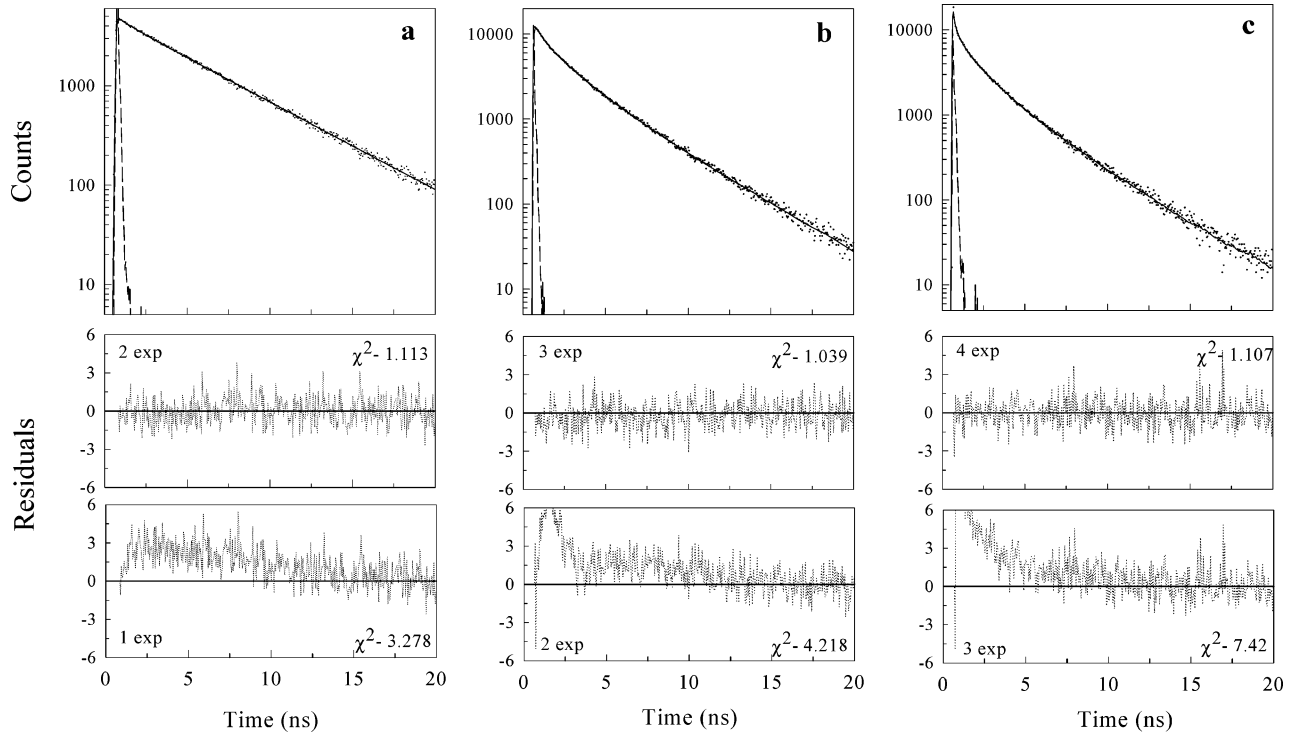

FIGURE 1: Fluorescence intensity decays of the different states of barstar (W38FW44F mutant): (a) N state (pH 7), (b) U form (6 M GdnHCl at pH 7), and (c) D form (pH 12). Excitation and emission wavelengths were 295 and 335 nm, respectively. The excitation profile (dashed line), the emission profile (dots), and the calculated emission profile (solid line) are shown. The goodness of fit is shown in panels below each decay profile, with the respective χ^2 values.

Table 1: Parameters Associated with the Decay of Fluorescence Intensity of W38FW44F at 25 °C[a]

experimental conditions											
pH	[GdnHCl] (M)	[Na_2SO_4] (M)	τ_1 (ns)	α_1	τ_2 (ns)	α_2	τ_3 (ns)	α_3	τ_4 (ns)	α_4	τ_m (ns)
7	0 (N state)	0	–	–	–	–	1.1	0.05	5.06	0.95	4.86
7	6 (U form)	0	–	–	0.29	0.26	1.53	0.38	3.61	0.36	1.97
12	0	0 (D form)	0.020	0.77	0.33	0.06	1.6	0.11	3.6	0.06	0.4
12	0	0.015	0.024	0.79	0.31	0.06	1.34	0.09	3.03	0.06	0.3
12	0	0.035	0.030	0.78	0.32	0.05	1.30	0.10	3.06	0.07	0.38
12	0	0.05	0.030	0.76	0.34	0.07	1.43	0.10	3.29	0.07	0.47
12	0	0.1	0.054	0.66	0.51	0.12	1.70	0.16	4.10	0.09	0.6
12	0	0.2	0.050	0.57	0.41	0.12	1.55	0.20	3.59	0.11	0.79
12	0	0.3	0.050	0.52	0.41	0.14	1.57	0.21	3.83	0.13	0.91
12	0	0.4	0.055	0.47	0.44	0.15	1.56	0.20	3.87	0.17	1.08
12	0	0.5	0.060	0.50	0.50	0.15	1.79	0.17	4.02	0.17	1.12
12	0	0.6	0.060	0.50	0.46	0.12	1.77	0.16	3.92	0.21	1.3
12	0	0.7	0.070	0.41	0.50	0.13	1.80	0.20	3.93	0.25	1.21
12	0	0.8	0.054	0.48	0.42	0.09	1.70	0.15	3.80	0.27	1.33
12	0	0.9	0.050	0.46	0.36	0.08	1.60	0.15	3.78	0.30	1.44
12	0	1.0 (B form)	0.067	0.44	0.43	0.10	1.67	0.17	3.82	0.30	1.5

[a] The χ^2 values were in the range of 0.95−1.2 for all the data. The errors in the values are ±5%, obtained from three independent experiments. τ_1−τ_4 are the fluorescence lifetimes. α_1−α_4 are the fractional amplitudes for the corresponding lifetimes. τ_m is the mean lifetime.

exponentials. The lifetimes and their corresponding amplitudes are as follows: 3.61 ns and 36.2%, 1.53 ns and 38.44%, and 0.3 ns and 25.36%, respectively. The mean lifetime ($\tau_m = \sum\alpha_i\tau_i$) decreases from 4.9 ns for the native protein with 0 M GdnHCl at pH 7 to 1.97 ns for the protein unfolded in 6 M GdnHCl at pH 7 (Table 1). While only three lifetime components can be observed for the U form, an additional, very short lifetime component (~77% amplitude) of ~40 ps is observed for the D form at pH 12. The fluorescence intensity decay of Trp53 in the D form fits best to four exponentials ($\chi^2 = 1.1$) as shown by the residuals (Figure 1c). The mean lifetime of Trp53 in the D form at pH 12 is ~0.4 ns, due to the predominant contribution from the ultrafast sub-nanosecond component. To rule out any pH dependence of the fluorescence lifetime of tryptophan, *N*-acetyl-l-tryptophanamide (NATA) was dissolved in pH 12 buffer, and its lifetime was measured. The lifetime of NATA changed from 2.8 ns at pH 7 to 2.4 ns at pH 12 (data not shown). Thus, the ultrafast (40 ps) component does not appear to be the result of an alteration of the fluorophore at high pH. It should be noted that the ratio of the mean lifetime of the N state to that of the D form predicts the observed ratio of steady-state fluorescence intensities. In the case of the U form, since the ultrafast lifetime component is too fast to be observed by the instrumentation that was used, the ratio of the steady-state fluorescence intensity of the N state to that of the U form is not predicted by the ratio of measured mean lifetimes.

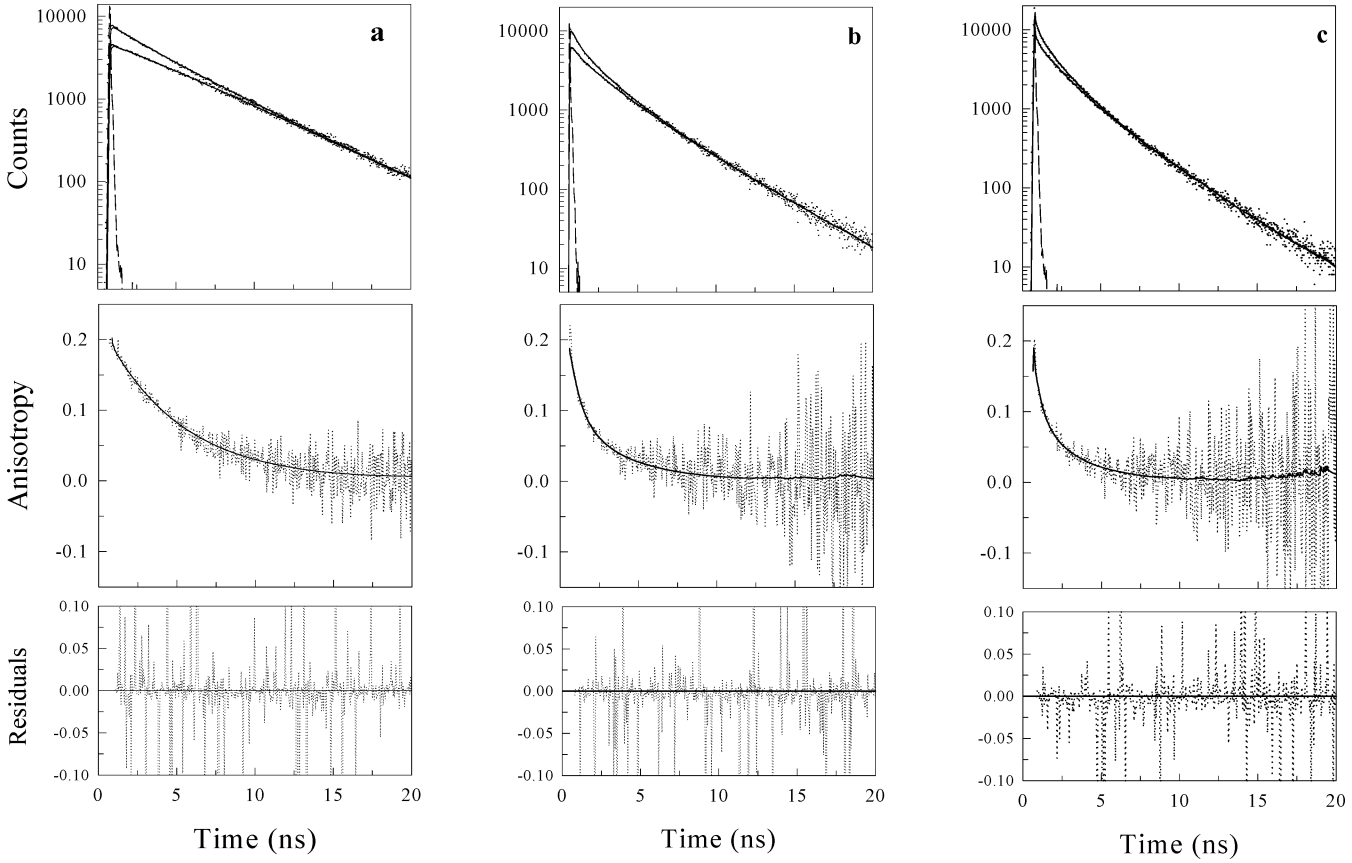

FIGURE 2: Decays of fluorescence anisotropy of the different states of barstar: (a) N state, (b) U form, and (c) D form. Excitation and emission wavelengths were 295 and 335 nm, respectively. The top panel in each case shows the fluorescence intensity decays from the parallel and perpendicular channels. The dots correspond to the raw data, and the solid line through the data represents the calculated emission profile. The middle panel in each case shows the anisotropy decay, calculated using eq 2. The dotted lines are the raw anisotropy decays, and the thick solid lines through the data correspond to the fitted lines obtained using eq 6. The bottom panels show plots of the residuals for estimating the goodness of fit. Detailed parameters are listed in Table 2.

The fluorescence lifetime of Trp53 in the D form was measured in the presence of different concentrations of the stabilizing salt Na_2SO_4. At all salt concentrations, the fluorescence intensity decay fits best to four exponentials. The observed lifetimes and their associated amplitudes are shown in Table 1. With increasing concentrations of Na_2SO_4 at pH 12, two changes are very apparent. (i) The contribution of the slowest lifetime component (~4 ns) to the overall intensity decay increases from ~6 to ~30%. This occurs primarily at the expense of the ultrafast (~40 ps) component whose amplitude decreases from ~77 to ~45%. (ii) The mean lifetime increases from ~0.4 ns at pH 12 with 0 M Na_2SO_4 to ~1.5 ns at pH 12 in 1 M Na_2SO_4.

Anisotropy Decay Measurements. Time-resolved fluorescence anisotropy decay measurements were carried out for barstar in the N state (pH 7), the U form (6 M GdnHCl at pH 7), the D form (pH 12), and the molten globule B form (1 M Na_2SO_4 at pH 12) to study the rotational dynamics of the Trp in different conformational states. In each case, the decay parameters that were obtained were averaged over three independent experiments. Typical examples of anisotropy decays for the different states of the protein are shown in Figure 2. The values obtained for τ_{r_1}, τ_{r_2}, β_1, and β_2, the χ^2 values, and the values obtained for the initial anisotropy (r_o) and steady-state anisotropy (r_{ss}) are summarized in Table 2. The reduced χ^2 value, a measure of the goodness of fit, was always less than 1.2, and the weighted residuals and the autocorrelation of the residuals show random distributions indicating an optimal fit.

Native protein at pH 7 displays a single rotational correlation time [$\tau_r \sim 5.1$ ns ($\chi^2 = 1.09$)] as shown in Figure 2a. The value of the initial anisotropy (r_o) is 0.2. In contrast to earlier observations (*33*, *56*), in which a single rotational correlation time of ~1.6 ns was observed for the U form, two rotational correlation times are observed for the U form in 6 M GdnHCl at pH 7. A long rotational correlation time (τ_{r_1}) of ~3.7 ns and a short rotational correlation time (τ_{r_2}) of ~0.7 ns are observed ($\chi^2 = 1.06$) with each component making an ~50% contribution to the total anisotropy decay (Figure 2b). Force fitting the same data to a single exponential results in a large nonrandom distribution of the data points about the fit and a high χ^2 value. The 2.2 and 1.6 ns rotational correlation times that were observed in earlier studies (*33*, *56*) for the urea- and guanidine hydrochloride-unfolded proteins, respectively, could have arisen from a weighted average of free side chain motion and segmental motion, which might have been unresolvable due to the quality of the data. The U form has an apparent value for r_o of 0.18, which is less than the value of 0.2 observed for the N state. The cone angle for restricted rotation, calculated using the value of β_1 using eq 8, gives a value of 39°.

Similarly, the anisotropy decay for the D form at pH 12 as shown in Figure 2c fits best to two exponentials ($\chi^2 = 1.11$). The observed long rotational correlation time (τ_{r_1}) of

Table 2: Parameters Associated with the Decay of Fluorescence Anisotropy of W38FW44F at 25 °C[a]

experimental conditions											
pH	[GdnHCl] (M)	[Na_2SO_4] (M)	τ_{r_1} (ns)	τ_{r_1}* (ns)	β_1	τ_{r_2} (ns)	β_2	r_o	r_{ss}	r_{ss}*	χ^2
7	0 (N state)	0	5.10	5.10	1.00	–	–	0.202	0.100	0.100	1.09
7	0	1.0	7.82	5.10	1.00	–	–	0.202	0.100	0.100	1.10
7	6 (U form)	0	3.67	2.25	0.49	0.76	0.51	0.180	0.072	0.070	1.10
12	0	0 (D form)	2.60	2.54	0.50	0.26	0.5	0.175	0.060	0.059	1.11
12	0	0.015	3.64	3.55	0.53	0.4	0.47	0.198	0.062	0.070	1.12
12	0	0.035	4.30	4.20	0.50	0.52	0.5	0.197	0.066	0.073	1.10
12	0	0.05	5.88	5.70	0.48	0.62	0.52	0.190	0.068	0.080	1.15
12	0	0.1	6.70	6.37	0.54	0.63	0.46	0.204	0.071	0.090	1.00
12	0	0.2	7.07	6.51	0.73	0.78	0.27	0.198	0.090	0.108	1.04
12	0	0.3	7.21	6.36	0.81	0.96	0.19	0.200	0.105	0.120	1.00
12	0	0.4	7.60	6.37	0.88	1.04	0.12	0.202	0.116	0.127	1.16
12	0	0.5	7.20	5.72	0.92	1.06	0.08	0.201	0.122	0.128	1.04
12	0	0.6 (I_{CC})	8.20	6.21	1.00	–	0.00	0.198	0.121	0.130	1.02
12	0	0.7	8.40	6.05	1.00	–	0.00	0.198	0.123	0.130	1.01
12	0	0.8	9.33	6.42	1.00	–	0.00	0.193	0.123	0.128	1.07
12	0	0.9	9.25	6.10	1.00	–	0.00	0.195	0.125	0.128	1.00
12	0	1.0 (B form)	9.38	6.11	1.00	–	0.00	0.198	0.123	0.127	1.08

[a] τ_{r_1} and τ_{r_2} are the observed rotational correlation times, and β_1 and β_2 are the corresponding fractional amplitudes. τ_{r_1}* is the viscosity-corrected value of the long rotational correlation time. r_o represents the initial anisotropy. r_{ss} and r_{ss}* represent the steady-state anisotropy values obtained from time-resolved anisotropy decay experiments using eq 7 and directly from steady-state measurements, respectively. The errors in the values are ±10%, obtained from three independent experiments.

2.6 ns and the short rotational correlation time (τ_{r_2}) of 0.26 ns contribute equally (~50%) to the total observable decay in anisotropy. Force fitting to a single exponential results in a large nonrandom distribution of the data about the fit and a high χ^2 value. The cone angle of rotation calculated using the value of β_1 is 35°. An r_o value of 0.175 for the D form is similar to the value for the U form (0.18) and less than the value for the N state (0.2). The values of r_o for the N, D, and U forms are considerably smaller than the expected value of 0.4.

Table 2 and Figure 3 show how the short and long rotational correlation times of the D form at pH 12 evolve with increasing salt concentration. Since the addition of 1 M Na_2SO_4 to a buffered solution at pH 7 or 12 increases the value of the relative viscosity to 1.53 at 25 °C (data not shown), and because the long rotational time (τ_{r_1}) of the N state, which is known to represent global tumbling motion (*56*), is observed to scale linearly with solution viscosity (unpublished results), the value of τ_{r_1} measured at each salt concentration, in the range of 0−1 M, was corrected using the value of the relative viscosity measured for each solution. Table 2 shows the uncorrected as well as viscosity-corrected values of τ_{r_1}. No similar correction has been carried out for the short rotational correlation time, τ_{r_2}, because that is known to represent local motion of the Trp53 side chain (*56*). The theory concerning the effect of bulk viscosity changes on segmental motion of a polypeptide chain and local rotational motion of an amino acid side chain is not well-understood. It should also be mentioned that the instrumentation that was used, whose instrument response function (IRF) has a half-width of ~40 ps, cannot properly distinguish any change occurring in a fluorescence anisotropy decay with a time constant of less than 100 ps. For example, the rotational correlation time of NATA in 1 M Na_2SO_4 at pH 12 was measured to be ~70 ps, similar to the value (~80 ps) measured in the absence of added salt at pH 12.

Figure 3 shows that the value of ~2.5 ns for the viscosity-corrected long correlation time (τ_{r_1}*) in the D form increases in value to ~6.4 ns upon addition of ~0.1 M Na_2SO_4 (Figure 3a). Between 0.1 and 1 M Na_2SO_4, the value of τ_{r_1}* remains constant at ~6 ns. Figure 3b shows the contribution of the slow and fast rotational events to the total observable decay in anisotropy, at each Na_2SO_4 concentration. In the 0−0.1

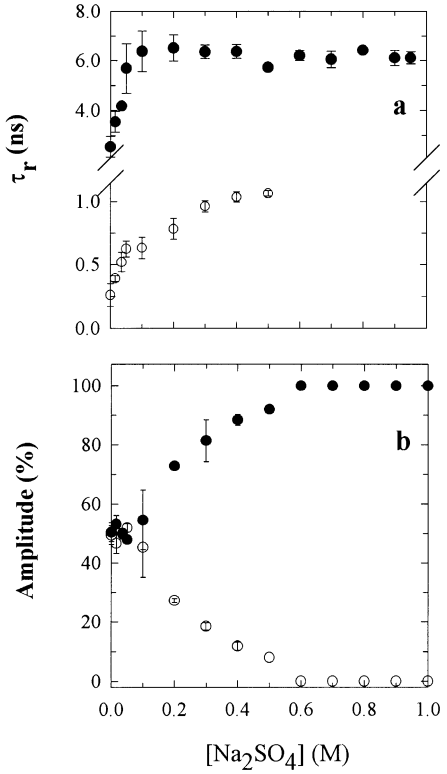

FIGURE 3: Rotational correlation times and amplitudes plotted as a function of Na_2SO_4 concentration. (a) Viscosity-corrected long correlation times, τ_{r_1}* (●), show an initial increase from ~2.5 to ~6.4 ns at 0.1 M Na_2SO_4. The values remain constant at higher salt concentrations. Short correlation times, τ_{r_2} (○), show a gradual increase from 0.26 to 1.1 ns at 0.5 M Na_2SO_4. The error bars are standard deviations obtained from three independent experiments. (b) Amplitudes of decay in anisotropy due to τ_{r_1} and τ_{r_2} [β_1 (●) and β_2 (○), respectively] are shown. Error bars represent standard deviations obtained from averaging over three independent experiments.

M Na_2SO_4 concentration range, where the maximum change in the value of τ_{r_1}* occurs, the amplitude corresponding to τ_{r_1}* (β_1) remains constant at ~50%. Beyond 0.1 M Na_2SO_4, the value of β_1 increases steadily and reaches 100% by ~0.6 M Na_2SO_4. Correspondingly, the amplitude corresponding to τ_{r_2}, β_2 (=1 − β_1), remains constant at ~50% in the 0−0.1 M Na_2SO_4 concentration range, and beyond 0.1 M Na_2SO_4, it decreases steadily in value to become negligible by ~0.6 M Na_2SO_4. Beyond 0.5 M Na_2SO_4 (pH 12), the anisotropy decay of Trp53 in the protein fits best to a single exponential (τ_{r_1}* ~ 6 ns). The value of τ_{r_2} increases from 0.26 ns in the D state to ~1.1 ns by 0.5 M Na_2SO_4 [Figure 3a (○)].

Several checks were carried out to test the uniqueness of the values of parameters obtained from fitting the data. (1) Force fitting the anisotropy decay data obtained at concentrations of Na_2SO_4 greater than 0.5 M to two exponentials did not improve the χ^2 values and also gives negative amplitudes for one of the decay components. Also, each τ_r was constrained to a value distant from that obtained by the free fit: the value obtained for χ^2 was much higher, and the residuals showed nonrandom distributions, indicating that the free fit yielded a unique value of τ_r. (2) Force fitting the anisotropy decay data obtained at each of the concentrations of Na_2SO_4 between 0 and 0.1 M to three exponentials was tried in several different ways, (a) with the three τ_r values fixed at ~0.26 ns (the value of τ_{r_2} in 0 M Na_2SO_4), ~2.6 ns (the value of τ_{r_1} in 0 M Na_2SO_4), and ~9 ns (the value of τ_{r_1} in 0.1−1 M Na_2SO_4) and only the amplitudes allowed to vary, (b) with one τ_r value fixed at ~2.6 ns and the other two τ_r values along with the three amplitudes allowed to vary, (c) with one τ_r value fixed at ~9 ns and the other two τ_r values along with the three amplitudes allowed to vary, and (d) with all three τ_r values along with all three amplitudes allowed to vary. The forced three-exponential fits resulted either in a bad fit or in a negative amplitude for one of the τ_r values, indicating that three-exponential fits do not yield stable and consistent values for the three rotational correlation times.

It must be mentioned that the value of the mean lifetime (τ_m) increases from 0.4 ns to only 1.5 ns during the entire (from 0 to 1 M Na_2SO_4) salt-induced folding transition. The fact that even the highest value (1.5 ns) measured for τ_m is much shorter than the highest value (~9 ns) measured for τ_r is potentially a point of concern in determining the value of the long rotational correlation time. This is because the information pertaining to the decay in anisotropy is contained in the difference between the parallel and perpendicular components of fluorescence emission. When τ_r = 2.6 ns and τ_m = 0.4 ns, the difference between the two components does not persist beyond ~1.2 ns, and when τ_r = 9 ns and τ_m = 1.5 ns, the difference does not persist beyond ~4.5 ns. Hence, determination of the rotational correlation times of the slow tumbling motion is associated with a greater inherent error due to under-representation in the intensity decay curves, while the faster motions are represented more accurately. Nevertheless, as seen in Figure 2c, the long rotational correlation times could be recovered with sufficient accuracy.

Dependences of Multiple Spectroscopic Properties on Na_2SO_4 Concentration. Figure 4 compares the dependences on Na_2SO_4 concentration of multiple steady-state and time-resolved spectroscopic properties of the protein at pH 12. The data collected using CD in the peptide (Figure 4a) and aromatic region (Figure 4b) as probes for secondary structure and tertiary structure have been taken from earlier studies (*21*). CD at 222 nm, which monitors α-helical secondary structure [Figure 4a (●)], and CD at 216 nm, which monitors β-sheet structure [Figure 4a (△)], show sigmoidal dependences on Na_2SO_4 concentration. CD at 275 nm, which measures the asymmetry in the environment around the aromatic residues, increases in value with increasing Na_2SO_4 concentration from 0 to 0.5 M Na_2SO_4, beyond which it saturates. The values for the steady-state tryptophan fluorescence intensity changes (Figure 4c) agree very well with the mean lifetime (τ_m) (Figure 4d) obtained from the set of experiments presented here. The values of r_{ss} determined directly from steady-state measurements (Figure 4e) agree well with the values determined from analysis of the time-resolved fluorescence anisotropy data (Table 2) and, hence, validate that analysis.

The absolute values of the hydrodynamic radius (R_H) as obtained from DLS are slightly different from those reported earlier (*21*) after we correct for a combination of pH and viscosity errors. The DLS experiments have been repeated, and the data are shown in Figure 4f. The trend of variation of R_H with Na_2SO_4 concentration remains the same as reported earlier. The value of R_H obtained for the D form at pH 12 now agrees with that expected from gel filtration, NMR, and other procedures.

Figure 5 shows that the transitions monitored by steady-state tryptophan fluorescence intensity, aromatic CD, and mean lifetime obtained from the time-resolved fluorescence experiment (Table 1), which are all probes for the gross tertiary fold, overlap well with each other within error. The transition monitored by steady-state anisotropy (r_{ss}) is not shown along with the transitions measured by the other probes, because unlike the latter, steady-state anisotropy is not solely a mole fraction-weighted signal; it scales as a function of mole fraction as well as of the relative quantum yields of the forms of the protein that is present (*56*). The buildup of secondary structure (α-helix and β-sheet) shows a distinct sigmoidal dependence on Na_2SO_4 concentration, which is markedly different from, and noncoincident with, other structural parameters.

Refolding Kinetics. In Figure 6, the kinetics of refolding at pH 7, when refolding was initiated from different initial conditions, are compared. Figure 6a shows the changes in tryptophan fluorescence intensity as a function of time, when refolding is initiated from different initial conditions, while Figure 6b shows the dependence of refolding rates on Na_2SO_4 concentration when refolding is initiated from different initial conditions. When refolding is initiated from the D form at pH 12, the major phase of refolding (85%) occurs at a rate of ~45 ± 5 s^{-1} and leads to the formation of the N state. The dependence of refolding rates on Na_2SO_4 concentration is nonlinear. The refolding rates increase to a value of ~100 s^{-1} (by ~0.5 M Na_2SO_4), following which the rates do not increase significantly up to 1 M Na_2SO_4. When refolding is initiated from the P form at 0.1 M Na_2SO_4 (pH 12), the refolding rates at low salt concentrations (<0.5 M Na_2SO_4) are marginally faster compared to the rate of folding from the D form. Refolding rates show a distinct nonlinear dependence on final salt concentration. When refolding is initiated from 0.6 M Na_2SO_4 (pH 12), it occurs at a rate of

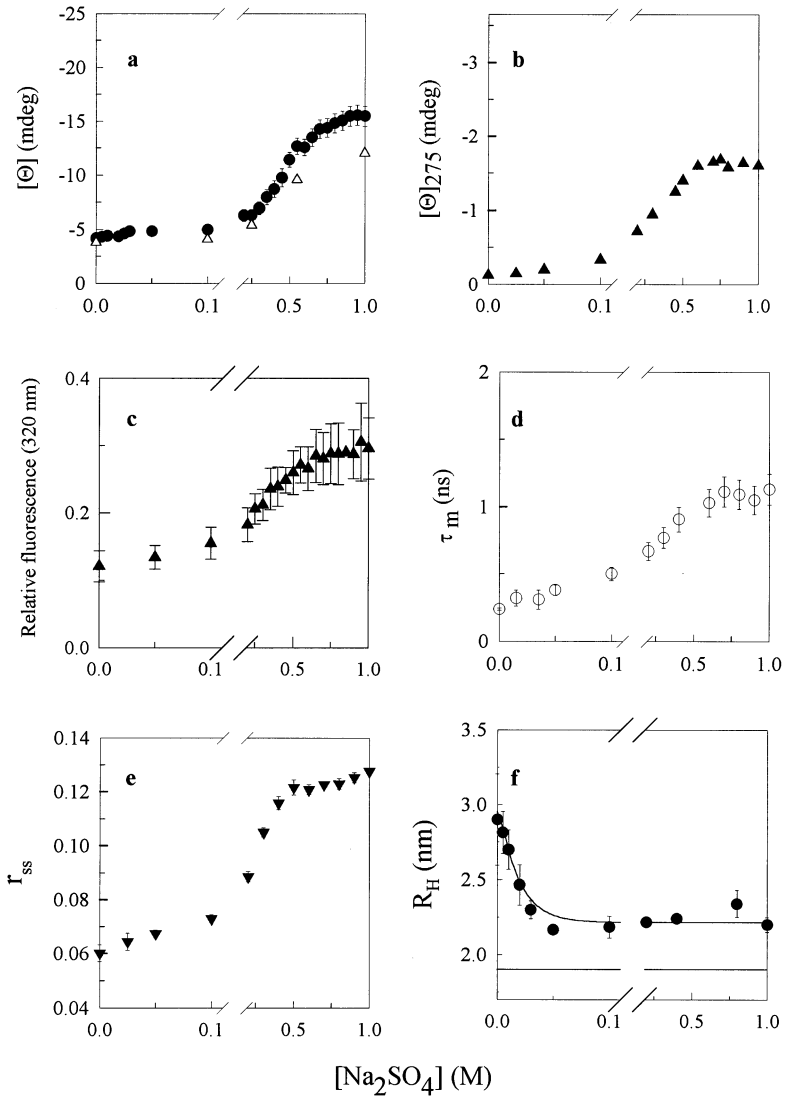

FIGURE 4: Raw values for the Na_2SO_4-induced structure acquisition in the D form as observed by multiple spectroscopic probes: (a) far-UV CD [222 nm (●) and 216 nm (△)], (b) near-UV CD (275 nm), (c) steady-state fluorescence intensity at 320 nm following excitation at 295 nm, (d) mean lifetime (τ_m), (e) steady-state anisotropy (r_{ss}), and (f) hydrodynamic radius (R_H).

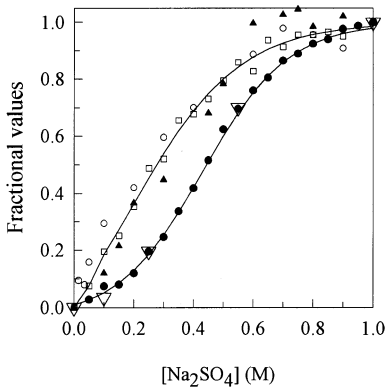

FIGURE 5: Fractional values of multiple structural probes: τ_m (○), near-UV CD (▲), steady-state Trp fluorescence intensity at 320 nm (□), and far-UV CD at 222 nm (●) and 216 nm (▽). The solid lines through the data are three-state fits to observed transitions (*21*).

~110 s^{-1} and is fast compared to refolding initiated from the D and P forms. Furthermore, the refolding kinetics do not depend on the final Na_2SO_4 concentration in the 0−1 M range. Similarly, when refolding is initiated from the B form at pH 12 with 1 M Na_2SO_4, it also show faster refolding rates (~125 s^{-1}), which are independent of the final salt concentration in the range of 0.1−1 M Na_2SO_4.

Modification of Protein at High pH. In the previous study of structure formation upon addition of Na_2SO_4 at pH 12, no chemical modification of the protein could be discerned by mass spectrometry carried out at pH 7. Mass spectrometry at pH 2 indicates, however, that the mass of the protein increases by ~1 Da, from 10 264.89 ± 0.12 to 10 266.14 ± 0.09 Da, when the protein at 100 μM is incubated at pH 12 for a period of 2−4 h. For the protein treated at pH 12, the observation of a mass increase of 1 Da for a sample at pH 2 and not for a sample at pH 7 suggests that deamidation of an Asn to an Asp or a Gln to a Glu in the protein occurs between hours 2 and 4 of the treatment at pH 12 (R. Sade, J. Nandakumar, and J. B. Udgaonkar, unpublished observations).

This chemical modification affects the stability of the protein measured at pH 7. After a 4 h incubation of 100 μM protein at pH 12, the midpoint of the GdnHCl-induced denaturation curve decreases from 1.75 M (whether measured by far-UV CD or fluorescence) to 1.2 ± 0.1 M when

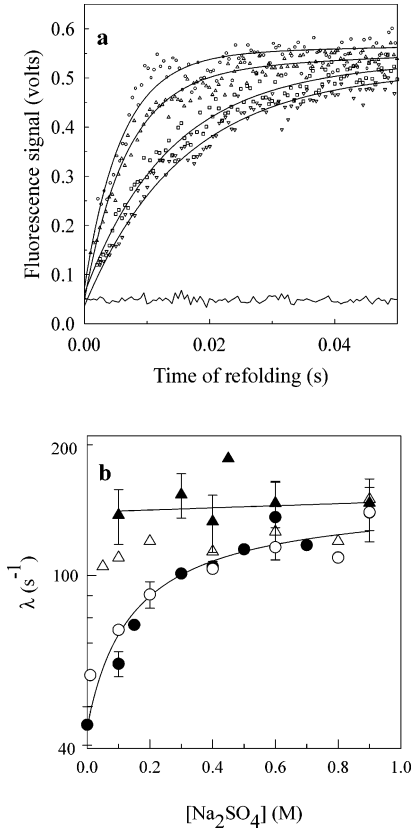

FIGURE 6: Core compaction is the rate-limiting step in the folding of barstar. (a) Refolding traces in 0.1 M Na_2SO_4 at pH 7 are shown when refolding is initiated from different initial conditions. The different symbols represent refolding initiated from the pH 12 unfolded D form (▽), the 0.1 M Na_2SO_4, pH 12 P form (□), the 0.6 M Na_2SO_4, pH 12 I_{CC} form (△), and the 1 M Na_2SO_4, pH 12 B form (○). (b) Refolding rates (fast phase) of the pH 12 unfolded D form (●), 1 M Na_2SO_4, pH 12 B form (▲), 0.1 M Na_2SO_4, pH 12 P form (○), and 0.6 M Na_2SO_4, pH 12 I_{CC} form (△) when refolded in different concentrations of Na_2SO_4 in the range of 0−1 M, at pH 7. The values represent the means, and the error bars represent the standard deviations from three separate experiments. The line through the data is a mere guide to the eye and does not represent any functional dependence of the observed rates on Na_2SO_4 concentration.

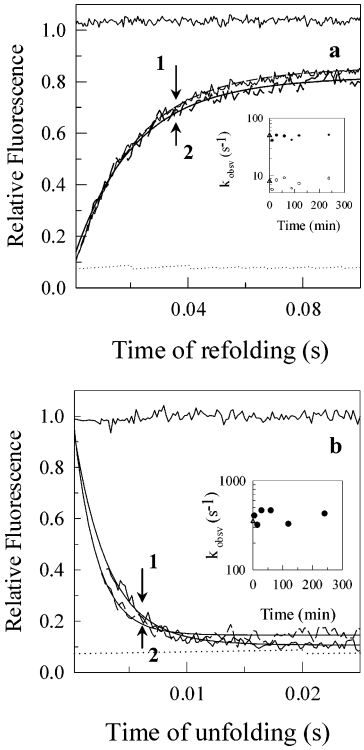

FIGURE 7: pH jump-induced refolding kinetics (a) and unfolding kinetics (b) are not significantly affected by chemical modification. The dotted line in each panel indicates the unfolded protein signal at pH 12; the native protein has a signal of 1. The solid line through the fluorescence intensity data indicates exponential fits to the data. The trace marked with a 1 in panel a represents the folding trace of protein treated at pH 12 for 15 s, and the trace marked with a 1 in panel b represents the unfolding trace of the untreated protein. The traces marked 2 in panels a and b represent the folding and unfolding traces of protein treated at pH 12 for 4 h. The inset in each panel indicates the scatter observed in the refolding (a) or unfolding (b) rates as a function of time of incubation at pH 12. The △ symbols in the inset of panel a indicate the fast and intermediate refolding rates of protein at pH 12 which had been unfolded at pH 12 for 15 s. The △ symbols in the inset of panel b indicate the unfolding rates of protein at pH 7 which had not been unfolded to pH 12.

monitored by fluorescence, and to 1.45 ± 0.05 M when monitored by CD (data not shown). Thus, the chemical modification leads to stabilization of an equilibrium unfolding intermediate, and converts barstar from a two-state to a three-state equilibrium unfolder (R. Sade and J. B. Udgaonkar, unpublished observations).

The chemical modification does not, however, have any effect on the reversibility of the folding or unfolding reaction. Complete fluorescence and CD signals corresponding to the N state are recovered upon refolding the pH 12 unfolded protein at pH 7 (*58*). Similarly, CD as well as fluorescence signals for the N and U states, observed during GdnHCl-induced unfolding transitions at pH 7, are the same for the protein that had been incubated previously at pH 12 for 4 h (at 100 μM) before being refolded at pH 7 and for protein that had not been incubated in such a way. Moreover, all structural probes used to characterize structure (Figures 1−4) gave identical signals whether the protein was incubated for 2 h (the minimum time for an equilibrium to be established) or 24 h under different conditions at pH 12.

Figure 7a shows that the refolding kinetics, following a jump in pH from 12 to 7, of barstar that had been unfolded at pH 12 for 4 h are virtually identical to the refolding kinetics of a protein that had been unfolded at pH 12 for only 15 s, and for which no chemical modification could be discerned by mass spectrometry. The inset of Figure 7a shows that the rates of the fast as well as intermediate phases of refolding, following jumps from pH 12 to 7, are not affected when the time of unfolding at pH 12 is changed from 15 s to 4 h. Figure 7b shows that the unfolding kinetics of barstar, following a jump in pH from 7 to 12, are very similar, within the range of error inherent in measurements of such fast rates, for a protein that had been previously refolded following a 4 h incubation at pH 12 and for protein that had not been incubated in such a way. The inset of Figure 7b shows that the very fast rate of unfolding, following a jump in pH from 7 to 12, is unaffected when the time of incubation at pH 12, prior to refolding, is increased to 4 h.

The results therefore suggest that the chemical modification, while affecting the stability of the protein at pH 7, has a negligible effect on the rates of the folding and unfolding

transitions effected by pH jumps, such as those reported in Figure 6. Thus, the chemical modification does not appear to affect the results presented in this study, and previously (*21*).

DISCUSSION

Fluorescence Lifetime Characteristics of Different Conformational States of Barstar. Under native conditions, the fully buried Trp53 displays two lifetimes of 5.06 (95%) and 1.1 ns (5%) as obtained by a discrete exponential analysis of the fluorescence intensity decay data. In contrast to the N state, the unfolded U form, in 6 M GdnHCl at pH 7, exhibits complex decay kinetics best approximated by three lifetime components. Steady-state spectroscopic probes (intrinsic Trp fluorescence, CD at 222, 216, and 275 nm) fail to detect any tertiary or secondary structure in the U form. Hydrodynamic probes (gel exclusion and dynamic light scattering) also suggest that the protein is in a highly extended state under such severe denaturing conditions (*21*). The observation of multiple lifetimes in the U form correlates with an increased flexibility of the polypeptide chain conformation. The presence of essentially a single lifetime for Trp53 in the N state suggests that Trp53 is locked in a single conformation (*59*). In the unfolded-state ensemble, the three rotamers of tryptophan probably experience different local environments which could govern the rate of quenching and give rise to multiple lifetimes. Alternately, dynamic processes such as spectral relaxation and/or resonance energy transfer (RET) can also lead to multiexponential decay.

The D form at pH 12 closely resembles the U form in being completely unfolded and lacking all aspects of structure (*58*). The additional ~40 ps component observed in the fluorescence intensity decay of the D form most likely represents an ultrafast, intrapolypeptide quenching process, as control experiments clearly indicate that the fast decay is not due to an alteration in the fluorescence properties of indole at high pH (see Results). At present, it is not possible to identify the quenching group.

With increasing Na_2SO_4 concentrations at pH 12, the contribution of the slowest component (~4 ns) to the fluorescence intensity decay increases (by ~25%) at the expense of the ultrafast (~40 ps) component. It appears that the generation of packing interactions during core formation causes the quenching group to move away from the tryptophan in a significant fraction of molecules, and hence, the contribution of quenching to the total decay is reduced. The buildup of the slowest decay component at the expense of the quenching component points toward the movement of the indole ring of Trp53 away from an environment that favors quenching to the conformational substate which has the longest lifetime. As a consequence, there is an increase in the mean lifetime (τ_m), which is coincident with the increase in steady-state fluorescence intensity as expected (Figure 5).

Motional Dynamics of Trp53 in the Different Conformational States of Barstar. In addition to being affected by size, the decay of fluorescence anisotropy in proteins is affected by shape and segmental flexibility (*60, 61*). Rotational correlation times that are too short to be approximated by overall rotational diffusion of a protein molecule have been attributed to independent motions of tryptophan residues within the protein. Short rotational correlation times provide invaluable information about the internal dynamics of proteins. The side chain of Trp53 is 99% buried in the core of native state of barstar as observed in both the crystal structure (*62*) and solution NMR structure (*63*). Studying the dynamics of such a Trp therefore allows a systematic characterization of core dynamics in the N state, in the D and B forms, and during the D $\rightleftharpoons$ B transition.

N State. The anisotropy decay of native barstar fits well to a single exponential, giving a long rotational correlation time of 5.1 ns. For a protein of ~10.1 kDa, a rotational correlation time of 5 ns can be accounted for only upon incorporation of a shell comprising two layers of tightly bound water molecules on the protein surface (*64*). The absence of a fast decay in anisotropy suggests that Trp53, located on β-strand 2 (β_2) with its indole side chain sandwiched between α-helix 1 (α_1) and β_2 in the hydrophobic core, lacks independent motion, and argues in favor of a tightly packed core region around Trp53. Trp53 therefore reports only on the global tumbling motion in the N state. NMR studies of the backbone ^{15}N relaxation dynamics of wild-type barstar have also determined the overall molecular tumbling correlation time to be 5.2 ns (*65*), in support of the time-resolved fluorescence anisotropy data.

The value of 0.2 for the initial anisotropy, r_o, of the N state is considerably smaller than the value of 0.27−0.35 observed in the case of Trp in a rigid environment such as polyvinyl alcohol film or propylene glycol (*66*−*68*) and the theoretical value of 0.4 expected for collinear absorption and emission dipoles. Sub-picosecond rotational dynamics (*50*), such as the vibration of the indole emission dipole within a rotameric potential well, are the most likely reason for the observed value of r_o being lower than the theoretical estimates.

Chemically Unfolded and High-pH Denatured Forms. The rotational freedom of Trp53 increases upon unfolding due to the disruption of structure and packing interactions in the protein core. The system loses fluorescence anisotropy much faster in the U and D forms than in the N state. The anisotropy decay reveals two characteristic motions of Trp53 in the unfolded form. A fast component, τ_{r_2}, of 0.26 ns for the D form and 0.7 ns for the U form contributes to ~50% decay in the anisotropy. Independent motions of tryptophan as observed for NATA in water or in short, unstructured peptides show short correlation times in the range of 50−500 ps (*63*, *69*, *70*). τ_{r_2}, which falls in this range of values, therefore appears to represent the local, rotational motion of Trp53 around the $C_\alpha-C_\beta$ bond in the extended polypeptide. This rotation appears, however, not to be fully unhindered, and is responsible for only a partial loss of anisotropy as reflected in the β_2 value (<1). In accordance with this, the cone angles for restricted rotation, calculated using eq 8, give a value of 35° for the D form and 39° for the U form. The second, slower decay component, τ_{r_1}*, which has a value of ~2.5 ns for the D form and 2.25 ns for the U form, is too small to represent the rotational dynamics of the entire polypeptide chain, and therefore presumably reports on segmental flexibility, which accounts for the remaining 50% of the amplitude of anisotropy decay. r_0 has a value of 0.175 in the D form and 0.18 in the U form, which is less than the value of 0.2 observed for the N state. This points to an increased loss of anisotropy through sub-picosecond

rotational events, because of the increased flexibility in the D and U forms.

Global Collapse Precedes Specific Structure Formation. Earlier dynamic light scattering and gel exclusion chromatographic studies had shown that the first step in the equilibrium folding of barstar at pH 12, upon addition of ~0.1 M Na_2SO_4, is a global collapse of the extended D form to the structure-less, pre-molten globule P form (*21*), presumably because of Debye screening of repulsive charges. Far-UV CD at 222 nm fails to detect any increase in helicity accompanying structural collapse, and far-UV CD at 216 nm fails to detect any formation of β-sheet. The steady-state fluorescence intensity of Trp53 indicates that Trp53 is as solvated in the collapsed form as it is in the D form. Near-UV CD at 275 nm indicates the absence of any specific tertiary structure in the P form. The collapse of the D form to the P form may be likened to DNA condensation (*71*) caused by modification of electrostatic interactions between DNA segments by a variety of chemical agents. The many types of noncovalent interactions that drive the process of DNA condensation, and the requirement of a collapsed state for biological function, make the process similar to the initial step in protein folding.

Global Collapse Precedes Consolidation of the Core. Table 2 and Figure 3 show how the rotational correlation times evolve with addition of Na_2SO_4 to the D form at pH 12. The longer rotational correlation time (τ_{r_1}*) of 2.54 ns (Table 2) in the D form which accounts for ~50% of the anisotropy decay at 0 M Na_2SO_4 and pH 12 increases to ~6.4 ns (Table 2) in the P form at ~0.1 M Na_2SO_4 and pH 12 (Figure 3a). The P form therefore has ~30% greater volume than the N state. The evolution of τ_{r_1}* that accompanies structural collapse of the polypeptide therefore reflects the emergence of a global tumbling motion from the coalescence of local segmental motions. This salt-induced global collapse of the polypeptide chain that occurs during the D → P transition is evident not only from measurements of the long rotational correlation time but also from DLS measurements.

τ_{r_2}, which represents local tryptophan motion, increases from 0.26 ns in the D form to 0.65 ns in the P form in 0.1 M Na_2SO_4 (Figure 3a), suggesting that the motion of Trp53 is weakly hindered. Most significantly, the contribution of the fast rotational motion of Trp53 to fluorescence anisotropy decay still persists at ~50%, a value similar to that observed for the D form (Figure 3b). This implies that the product of the global collapse is a swollen, globular form with a highly fluid interior. The interior of the collapsed state permits free tryptophan motion, suggesting that it lacks any long-lived side chain packing interactions, and that it is a nonspecifically collapsed, dynamic form with high entropy. The above results provide the most direct view of the internal dynamics of the collapsed form that other studies failed to highlight. The results also agree well with the steady-state tryptophan fluorescence spectra obtained for the D and the P forms (*21*). The D and P forms have comparable fluorescence intensities at 320 nm, suggesting that Trp53 is equally solvent-exposed in both the cases. The λ_{max} shifts from 355 nm for the D form to 352 nm for the P form, suggesting a small change in the hydrophobicity of the environment around Trp53 (*21*).

Nature of Polypeptide Chain Collapse. The nature of the transition that governs polymer collapse and the requirement of a collapse event for correct folding of a polypeptide (*72*, *73*) are poorly understood. For proteins, the collapse of an extended chain into a limited volume can bring to the fore the excluded volume effects of side chains, thereby severely limiting the number of side chain conformations accessible for sampling (*47*, *49*). It appears, however, that a large number of non-native φ and ψ angles (or main chain conformations) can exist even in the relatively compact conformations of a collapsed ensemble, resulting in the entropy of the system (*49*) being larger than that of the N state. It has been suggested that the thermodynamics and kinetics of polypeptide collapse should depend on the net charge and salt concentration (electrostatic screening) of the system (*74*). It is therefore likely that the electrostatic repulsion in the D form at pH 12 impedes collapse, until the charges are screened by cations to facilitate chain contraction. Short-range hydrophobic interactions, in local clusters of nonpolar residues, are probably responsible for stabilizing the collapsed state with no hydrophobic core (*74*, *75*). In this context, lattice model studies have suggested that a net increase in the attraction between residues facilitates folding through an obligatory, rapidly collapsed, structure-less globule (*72*, *76*, *77*).

A fundamental question in protein folding studies is whether the initial collapse reaction is a cooperative two-state transition (*24*), or whether it is a continuous transition occurring through progressively more compact forms as envisaged for homopolymers. In the case of cytochrome *c*, the initial collapse of the polypeptide chain from the extended state appears to be a two-state process defined by a free energy barrier (*78*, *79*), whose origin is postulated to lie in the conformational entropy loss occurring during collapse. In the case of isocytochrome, compact as well as extended conformations appear to coexist in the very early stages of folding, and extended conformations persist until ~500 ms of folding (*80*). Heterogeneity in the initial collapse reaction had also been demonstrated previously in kinetic studies of the folding of barstar (*81*, *82*), lysozyme (*83*), and ribonuclease A (*84*).

In the equilibrium folding studies reported here, it is seen that during the D ⇌ P transition, the long rotational time (τ_{r_1}*) appears to increase gradually from 2.54 to 6.4 ns as the Na_2SO_4 concentration is increased from 0 to 0.1 M. If this transition is two-state, then the D and P forms should coexist over this range of salt concentrations. The fluorescence anisotropy decays should then have contributions from both forms of the proteins, and the observed (uncorrected) rotational correlation times characteristic of the D form (2.6 and 0.26 ns) and P form (~9 ns) would be observable at each salt concentration over which the D ⇌ P transition occurs, with only the amplitudes changing. The fluorescence anisotropy decays could not, however, be satisfactorily fit (see Results) to three exponentials that would indicate the coexistence of the D and P forms, suggesting therefore that the D ⇌ P transition is not two-state, but is instead a gradual continuous transition. It should, however, be noted that the limitations imposed on the analysis by the signal-to-noise ratio in the data may be the trivial reason three-exponential fits, in which the rotational correlation times are constrained to the values expected for the D and P forms, do not work.

Core Compaction Follows Collapse and Precedes Completion of Structure Acquisition. Between 0.1 and 1 M Na_2-

SO_4, the value of τ_{r_1}* remains constant at ~6 ns. The volume of the protein (a measure of the overall dimensions) therefore remains ~30% greater than that of the N state, a result that is in close agreement with earlier steady-state measurements. With increasing Na_2SO_4 concentrations, the value of τ_{r_2}, however, increases from 0.26 to 1.1 ns in 0.5 M Na_2SO_4. The fast motion of Trp53 is considerably restricted, and contributes to only ~10% of the observable decay in anisotropy at 0.5 M Na_2SO_4. In sharp contrast, the acquisition of secondary structure and tertiary contacts corresponding to the molten globule B form is complete only by 1 M Na_2SO_4 (Figure 5), which suggests that the core is consolidated before the complete acquisition of other global structural features corresponding to the B form.

The increase in the value of τ_{r_2} [Figure 3a (○)] and a reduction in its contribution to the observable decay in fluorescence anisotropy [Figure 3b (○)] suggest that the environment of the indole side chain of Trp53 becomes increasingly rigid with an increase in Na_2SO_4 concentration. Progressive consolidation of the hydrophobic core, through the formation of inter-residue packing interactions, is complete at 0.6 M Na_2SO_4. Complementary, albeit low-resolution, evidence had come from earlier steady-state tryptophan fluorescence spectra. The λ_{max} of 355 nm of the D form changes gradually to 330 nm by 1 M Na_2SO_4 with the maximum change occurring in the Na_2SO_4 concentration range of 0−0.6 M. With a net increase in hydrophobicity accompanying core compaction, as the Na_2SO_4 concentration is increased, water is progressively excluded from the core (*21*). The result that water expulsion and consolidation of the hydrophobic core of the protein occur after structural collapse finds parallels in theoretical predictions: using a SH3 protein model, it was shown that water expulsion occurs from the hydrophobic core region only after an initial structural collapse (*85*).

Rate-Limiting Step in the Folding of Barstar: Evidence for a Nucleation−Condensation Mechanism. Earlier kinetic studies, in which the kinetics of refolding of the fully unfolded D form at pH 12 to the N state at pH 7 had been compared to the kinetics of refolding of the molten globule B form at pH 12 to the N state at pH 7, had shown conclusively that the B form is an intermediate on the pathway of folding from the D form to the N state (*21*). The formation of well-defined tertiary contacts, which is possible only upon acquisition of tight side chain packing, characterizes the transition from the B form to the N state. As monitored by intrinsic tryptophan fluorescence, this transition occurs on a fast time scale and, hence, is not an inherently slow process. The rate-limiting barrier in protein folding must be found in other factors, and must also occur earlier, before an organized molten globule form is reached. In fact, the difference in the refolding kinetics of the D form and the B form (*21*) suggests that the rate-limiting barrier in the D ⇌ B → N reaction is encountered during the D ⇌ B transition. Thus, the B form is an on-pathway folding intermediate that is populated after the rate-limiting transition state of folding (Figure 8).

To assess the contribution of structural events that occur during the D ⇌ B transition to the rate-limiting barrier for folding, refolding kinetics starting from different initial conditions were compared (Figure 6). Refolding rates observed when folding is initiated from the structure-less, collapsed P form are only marginally faster than the rates observed when folding is initiated from the D form, suggesting that the loss of conformational entropy, which occurs during the D ⇌ P transition, does not contribute solely to the height of the barrier. On the other hand, the loss of conformational entropy accompanying the D ⇌ P transition may not be significant, if only the backbone configuration of the P form is relatively constrained, while the side chains remain highly disordered (see above). When refolding is initiated from protein at 0.6 M Na_2SO_4 and pH 12, the refolding kinetics are invariant to salt concentration and show a rate of ~110 s^{-1}, which is similar to the rate observed when folding is initiated from the B form in 1 M Na_2SO_4 (~125 s^{-1}). The form of the protein populated at 0.6 M Na_2SO_4 and pH 12, (I_{CC}) is a swollen, globally collapsed state with a rigid core, along with ~30% of the secondary structure and tertiary contacts of the native state. The acquisition of these structural features, during the P ⇌ I_{CC} transition, results in a gross, highly dynamic, native-like topology, and appears to be the major constitutive barrier to folding (Figure 8). Once a folding nucleus with a rigid core is formed, it appears to act as a nucleation center, and to facilitate further condensation of other regions of the polypeptide to form the native structure (*86*). At present, it is not possible to evaluate quantitatively the contributions of individual structural events to the barrier crossing process. What seems certain is that the loss of conformational entropy that occurs during the initial collapse and the consolidation of the protein core, which follows, are obligatory components of the rate-limiting barrier to folding (Figure 8). It is likely that the ~30% secondary structure observed in the intermediate with a compact core (I_{CC}) is thermodynamically favored by virtue of being in a collapsed, compact species (*87*).

On the basis of a more indirect protein engineering approach (*88*−*90*), a nucleation−condensation model had been proposed earlier for the folding of barstar, according to which hydrophobic core formation occurs late in folding. In those studies, the initial structural changes during folding were seen in the N-terminal $helix_1$−$loop_1$−$strand_1$ motif, presumably a direct consequence of the residual structure already present in the cold denatured state from which folding was initiated. The results reported here are therefore different from the results of the earlier protein engineering studies.

Similarities between the Equilibrium and Kinetic Folding Pathways of Barstar. Previously, stopped-flow kinetic measurements of the folding of barstar under marginally stable conditions had shown that an initial, apparently nonspecific hydrophobic collapse leads to the formation of a collapsed, structure-less globule intermediate, I_E (*27*), which precedes the formation of a molten globule-like intermediate on the folding pathway. Sub-millisecond folding studies, initiated by *T* jumps from the cold denatured state of barstar, have also shown the formation of an early intermediate, which is collapsed but with solvent-exposed side chains possessing high mobility (*88*, *89*). Evidently, the kinetic intermediate, I_E, shares many features in common with the equilibrium pre-molten globule P form, whose properties have been described in detail above. More recently, it has been shown that I_E is a heterogeneous ensemble of structures, and that different salts differentially stabilize different components of the I_E ensemble (*82*). At present, the degree of structural heterogeneity in the collapsed P form is unknown.

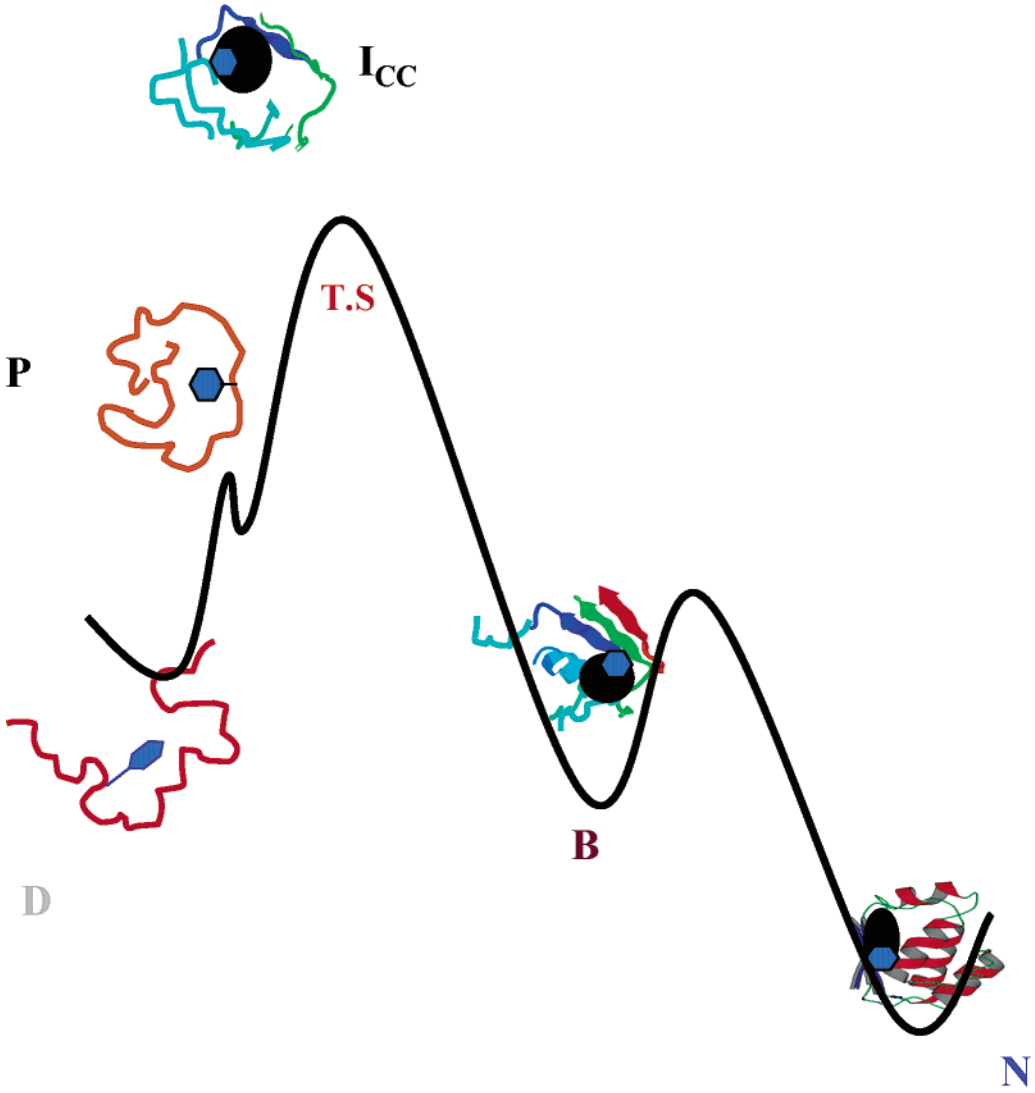

FIGURE 8: Nucleation−condensation model of folding of barstar. The placement of various intermediates with respect to the rate-limiting step for folding at pH 7 is highlighted. The black circles depicted in the intermediate with the compact core (I_{CC}), the MG form (B), and the native state (N) represent the tightly packed core of the protein. The blue hexagons depicted in each form represent the tryptophan residues.

Kinetic studies have also shown that I_E transforms into a late intermediate I_L (*81*, *91*). Under marginally stable conditions, I_L possesses little secondary structure, no tertiary interactions, exposed hydrophobic patches, a global tumbling time of 7.2 ns, and a free motion of Trp53 of ~1 ns (*33*). During the slow folding reaction of I_L to N, the free motion of Trp53 (~1 ns) disappears faster than the acquisition of other structural features (*33*), suggesting that this late reaction is itself not two-state. In the equilibrium studies reported here, in a process analogous to the progress of the slow folding reaction, the local motion of Trp53 is hindered progressively during the P ⇌ I_{CC} transition, as the core consolidates with increasing salt concentrations, and Trp53 becomes rigidly buried as the molecules transform into I_{CC} in 0.6 M Na_2SO_4. The global tumbling time of I_L is similar to the global tumbling times of the equilibrium P form, I_{CC}, and the B form, and the local tumbling time of the Trp53 side chain in I_L is similar to that seen during the P ⇌ I_{CC} transition, just before the side chain motion becomes frozen in I_{CC}. As also seen in the kinetic studies (*33*), core compaction is complete before secondary and tertiary structure formation corresponding to the molten globule B form is accomplished. Real-time NMR folding studies have shown that I_L is not a unique intermediate, but represents an ensemble of partly folded forms accumulating on multiple folding pathways (*92*). At present, there is no indication of whether the equilibrium intermediate forms studied here, including the P and B forms, similarly represent ensembles of partially folded forms that interconvert through a multitude of folding pathways.

CONCLUSIONS

This study of the dynamics of the transition between the unfolded form and the molten globule form analyzes each step in the process. The following is shown. (1) The fluctuating random coil structure in the D form undergoes a global collapse while retaining a highly fluid core. (2) The D form does not coexist with the collapsed form; i.e., all molecules collapse. (3) The collapsed form is swollen, highly hydrated with a volume that is 30% larger than that of the N state, and is devoid of any specific structure. (4) Core compaction (hydrophobic core formation) follows global collapse. (5) Core compaction precedes completion of specific structure acquisition. (6) The B form retains the

~30% greater volume compared to that of the N state, indicating that it is an expanded, dynamic structure with a compact, dry core. (7) The equilibrium and kinetic folding mechanisms of barstar appear to be similar. (8) Formation of a native-like topology, in a collapsed species that has a compact core and ~30% secondary and tertiary structure, constitutes the rate-limiting transition state in the folding pathway of barstar.

ACKNOWLEDGMENT

We thank Prof. N. Periasamy for providing the software used in the analysis of time-resolved fluorescence data and A. S. R. Koti for help with use of the TCSPC setup.

REFERENCES

1. Tanford, C. (1968) *Adv. Protein Chem. 23*, 121−275.
2. Ptitsyn, O. B. (1992) The molten globule state in Protein folding, *Dokl. Akad. Nauk SSSR 210*, 1213−1215.
3. Hamada, D., Hoshino, M., Kataoka, M., Fink, A. L., and Goto, Y. (1993) *Biochemistry 32*, 10351−10358.
4. Bai, Y., Sosnick, T. R., Mayne, L., and Englander, S. W. (1995) *Science 269*, 192−197.
5. Englander, S. W (1998) *Trends Biochem. Sci. 23*, 378.
6. Chamberlain, A. K., and Marqusee, S. (2000) *Adv. Protein Chem. 53*, 283−328.
7. Kuwajima, K. (1977) *J. Mol. Biol. 114*, 241−258.
8. Arai, M., and Kuwajima, K. (1996) *Folding Des. 1*, 275−287.
9. Gladwin, S. T., and Evans, P. A. (1996) *Folding Des. 1*, 407−417.
10. Kuwajima, K., Hiraoka, Y., Ikeguchi, M., and Sugai, S. (1985) *Biochemistry 24*, 874−881.
11. Kuwajima, K., Yamaya, H., Miwa, S., Sugai, S., and Nagamura, T. (1987) *FEBS Lett. 221*, 115−118.
12. Chaffotte, A. F., Cadieux, C., Guillou, Y., and Goldberg, M. E. (1992) *Biochemistry 31*, 4303−4308.
13. Goldberg, M. E., Semisotonov, G. V., Frituet, B., Kuwajima, K., Ptitsyn, O. B., and Sugai, S. (1990) *FEBS Lett. 263*, 51−56.
14. Sugawara, T., Kuwajima, K., and Sugai, S. (1991) *Biochemistry 30*, 2698−2706.
15. Kuwajima, K., Garvey, E. P., Finn, B. E., Matthews, C. R., and Sugai, S. (1991) *Biochemistry 30*, 7693−7703.
16. Dolgikh, D. A., Gilmanshin, R. I., Brazhnikov, E. V., Bychkova, V. E., Semisotonov, G. V., Venyamnov, S. Y., and Ptitsyn, O. B. (1981) *FEBS Lett. 136*, 311−315.
17. Goto, Y., and Fink, A. L. (1989) *Biochemistry 28*, 945−952.
18. Kuwajima, K. (1989) *Proteins: Struct., Funct., Genet. 6*, 87−103.
19. Ohgushi, M., and Wada, A. (1983) *FEBS Lett. 164*, 21−24.
20. Ptitsyn, O. B. (1992) in *Protein Folding* (Creighton, T. E., Ed.) pp 243−300, Freeman, New York.
21. Rami, B. R., and Udgaonkar, J. B. (2002) *Biochemistry 41*, 1710−1716.
22. Dill, K. A., and Stigter, D. (1995) *Adv. Protein Chem. 46*, 59−104.
23. Finkelstein, A. V., and Shakhnovich, E. I. (1989) *Biopolymers 28*, 1681−1689.
24. Chan, H. S., and Dill, K. A. (1991) *Annu. Rev. Biophys. Biophys. Chem. 20*, 447−490.
25. Richards, F. M. (1977) *Annu. Rev. Biophys. Bioeng. 6*, 151−176.
26. Richards, F. M., and Lim, W. A. (1993) *Q. Rev. Biophys. 26*, 423−498.
27. Agashe, V. R., Shastry, M. C. R., and Udgaonkar, J. B. (1995) *Nature 377*, 754−757.
28. Sosnick, T. R., Mayne, L., and Englander, S. W. (1996) *Proteins: Struct., Funct., Genet. 24*, 413−426.
29. Chan, C. K., Hu, Y., Takahashi, S., Rousseau, D. L., Eaton, W. A., and Hofrichter, J. (1997) *Proc. Natl. Acad. Sci. U.S.A. 94*, 1779−1784.
30. Sosnick, T., Shtilerman, M. D., Mayne, L., and Englander, S. W. (1997) *Proc. Natl. Acad. Sci. U.S.A. 94*, 8545−8550.
31. Lorch, M., Mason, N. M., Clarke, A. R., and Parker, M. J. (1999) *Biochemistry 38*, 1377−1385.
32. O'Neill, J., Jr., and Matthews, C. R. (2000) *J. Mol. Biol. 295*, 737−744.
33. Sridevi, K., Juneja, J., Bhuyan, A. K., Krishnamoorthy, G., and Udgaonkar, J. B. (2000) *J. Mol. Biol. 302*, 479−495.
34. Shastry, M. C., and Roder, H. (1998) *Nat. Struct. Biol. 5*, 385−392.
35. Colon, W., Elove, G. A., Wakem, L. P., Sherman, F., and Roder, H. (1996) *Biochemistry 35*, 5538−5549.
36. Northey, J. G. B., Di Nardo, A. A., and Davidson, A. R. (2002) *Nat. Struct. Biol. 9*, 126−130.
37. Kragelund, B. B., Osmark, P., Neergaard, T. B., Jacob, S., Kristiansen, K., Knudsen, J., and Poulsen, F. M. (1999) *Nat. Struct. Biol. 6*, 594−601.
38. Jackson, S. E., El Masry, N., and Fersht, A. R. (1993) *Biochemistry 32*, 11270−11278.
39. Plaxco, K. W., Simons, K. T., and Baker, D. (1998) *J. Mol. Biol. 277*, 985−994.
40. Riddle, D. S., Grantacharova, V. P., Santiago, J. V., Alm, E., Ruczinski, I., and Baker, D. (1999) *Nat. Struct. Biol. 6*, 1016−1024.
41. Martinez, J. C., and Serrano, L. (1999) *Nat. Struct. Biol. 6*, 1010−1016.
42. Chiti, F., Taddei, N., White, P. M., Bucciantini, M., Magherini, F., Stefani, M., and Dobson, C. M. (1999) *Nat. Struct. Biol. 6*, 1005−1009.
43. Fersht, A. R. (2000) *Proc. Natl. Acad. Sci. U.S.A. 97*, 1525−1529.
44. Matthews, B. W. (1987) *Biochemistry 26*, 6885−6888.
45. Lim, W. A., and Sauer, R. T. (1989) *Nature 339*, 31−36.
46. Matouschek, A., Kellis, J. T., Serrano, L., and Fersht, A. R. (1989) *Nature 340*, 122−126.
47. Behe, M. J., Lattman, E. E., and Rose, G. D. (1991) *Proc. Natl. Acad. Sci. U.S.A. 88*, 4195−4199.
48. Novotny, J., Rashin, A. A., and Bruccoleri, R. E. (1988) *Proteins 4*, 19−30.
49. Kussell, E., Shimada, J., and Shakhnovich, E. I. (2001) *J. Mol. Biol. 311*, 183−193.
50. Tcherkasskaya, O., Ptitsyn, O. B., and Knutson, J. R. (2000) *Biochemistry 39*, 1879−1889.
51. Bilsel, O., Yang, L., Zitzewitz, J. A., Beecham, J. M., and Matthews, C. R. (1999) *Biochemistry 38*, 4177−4187.
52. Chakraborty, S., Ittah, V., Bai, P., Luo, L., Haas, E., and Peng, Z. (2001) *Biochemistry 40*, 7228−7238.
53. Swaminathan, R., Periasamy, N., Udgaonkar, J. B., and Krishnamoorthy, G. (1994) *J. Phys. Chem. 98*, 9270−9278.
54. Nath, U., and Udgaonkar, J. B. (1997) *Biochemistry 36*, 8602−8610.
55. Khurana, R., and Udgaonkar, J. B. (1994) *Biochemistry 33*, 106−115.
56. Swaminathan, R., Nath, U., Udgaonkar, J. B., Periasamy, N., and Krishnamoorthy, G. (1996) *Biochemistry 35*, 9150−9157.
57. Kinoshita, K. J., Kawato, S., and Ikegami, A. (1977) *Biophys. J. 20*, 289.
58. Rami, B. R., and Udgaonkar, J. B. (2001) *Biochemistry 40*, 15267−15279.
59. Swaminathan, R., Krishnamoorthy, G., and Periasamy, N. (1994) *Biophys. J. 67*, 2013−2023.
60. Rischel, C., Thyberg, P., Rigler, R., and Poulsen, F. M. (1996) *J. Mol. Biol. 257*, 877−885.
61. Ross, J. B. A., Rousslang, K. W., and Brand, L. (1981) *Biochemistry 20*, 4361−4369.
62. Guillet, V., Lapthorn, A., Hartley, R. W., and Mauguen, Y. (1993) *Structure 1*, 165−176.
63. Lubienski, M. J., Bycroft, M., Freund, S. M. V., and Fersht, A. R. (1994) *Biochemistry 33*, 8866−8877.
64. Lakowicz, J. R. (1999) *Principles of fluorescence spectroscopy*, Chapters 16 and 17, Kluwer Academic/Plenum Publishers, Dordrecht, The Netherlands.
65. Sahu, S. C., Bhuyan, A. K., Majumdar, A., and Udgaonkar, J. B. (2000) *Proteins 41*, 460−474.
66. Valuer, B., and Weber, G. (1977) *Photochem. Photobiol. 25*, 441−444.
67. Ruggiero, A. J., Todd, D. C., and Fleming, G. R. (1990) *J. Am. Chem. Soc. 112*, 1003−1014.
68. Eftink, M. R., Gryczynski, I., Wiczk, W., Laczko, G., and Lakowicz, J. R. (1991) *Biochemistry 30*, 8945−8953.
69. Kouyama, I., Kinosita, K., and Ikegami, A. (1989) *Eur. J. Biochem. 182*, 517−521.
70. Chen, L. X.-Q., Petrich, J. W., Fleming, G. R., and Perico, A. (1987) *Chem. Phys. Lett. 139*, 55.
71. Bloomfield, V. A. (1997) *Biopolymers 44*, 269−282.

72. Gutin, A. M., Abkevich, V. I., and Shakhnovich, E. I. (1995) *Biochemistry 34*, 3066−3076.
73. Noppert, A., Gast, K., Zerwer, D., and Damaschun, G. (1998) *Folding Des. 3*, 213−221.
74. Stigter, D., Alonso, D. O. V., and Dill, K. A. (1991) *Proc. Natl. Acad. Sci. U.S.A. 88*, 4176−4180.
75. Tcherkasskaya, O., and Ptitsyn, O. B. (1999) *FEBS Lett. 455*, 325−331.
76. Sali, A., Shakhnovich, E., and Karplus, M. (1994) *Nature 369*, 248−251.
77. Dinner, A. R., Sali, A., and Karplus, M. (1996) *Proc. Natl. Acad. Sci. U.S.A. 93*, 8356−8361.
78. Hagen, S. J., and Eaton, W. A. (2000) *J. Mol. Biol. 301*, 1019−1027.
79. Hagen, S. J., and Eaton, W. A. (2000) *J. Mol. Biol. 297*, 781−789.
80. Lyubovitsky, J. G., Gray, H. B., and Winkler, J. R. (2002) *J. Am. Chem. Soc. 124*, 5481−5485.
81. Shastry, M. C., and Udgaonkar, J. B. (1995) *J. Mol. Biol. 247*, 1013−1027.
82. Pradeep, L., and Udgaonkar, J. B. (2002) *J. Mol. Biol. 324*, 331−347.
83. Morgan, C. J., Miranker, A., and Dobson, C. M. (1998) *Biochemistry 37*, 8473−8480.
84. Houry, W. A., and Scheraga, H. A. (1996) *Biochemistry 35*, 11734−11746.
85. Cheung, M. S., Garcia, A., and Onuchic, J. N. (2002) *Proc. Natl. Acad. Sci. U.S.A. 99*, 685−690.
86. Kussell, E., Shimada, J., and Shakhnovich, E. I. (2001) arXiv: cond-mat/0108357v1.
87. Chan, H. S., and Dill, K. A. (1990) *Proc. Natl. Acad. Sci. U.S.A. 87*, 6388−6392.
88. Nolting, B., Golbik, R., and Fersht, A. R. (1995) *Proc. Natl. Acad. Sci. U.S.A. 92*, 10668−10672.
89. Nolting, B., Golbik, R., Neira, J. L., Soler-Gonzalez, A. S., Schreiber, G., and Fersht, A. R. (1997) *Proc. Natl. Acad. Sci. U.S.A. 94*, 826−830.
90. Nolting, B. (1998) *J. Theor. Biol. 194*, 419−428.
91. Schreiber, G., and Fersht, A. R. (1993) *Biochemistry 32*, 5145−5150.
92. Bhuyan, A. K., and Udgaonkar, J. B. (1999) *Biochemistry 38*, 9158−9168.

BI030006B